ISSN : 2350-0743

International Journal of Recent Advances in Multidisciplinary Research

Vol. 12, Issue 12, pp.12018-12021, December, 2025
https://doi.org/10.64485/ijramr.6067.12.2025

RESEARCH ARTICLE

EFFECT OF TIAL INTERMEDIATE LAYER ON THE ADHESION STRENGTH OF TIALN COATINGS PREPARED BY ARC ION DEPOSITION (AIP)

Song Hyok Han[1,*], Chen Nam Kim[2], Hyon Gyu Pak[3], Nam Chol Yu[1*]

[1]Kim Chaek University of Technology, Pyongyang, Democratic People's Republic of Korea
[2]University of Science, Pyongyang, Democratic People's Republic of Korea
[3]RiKyeSun University of Education, North Huanghae, Democratic People's Republic of Korea

ARTICLE INFO

Article History
Received 24th September, 2025
Received in revised form
10th October, 2025
Accepted 15th November, 2025
Published online 29th December, 2025

Keywords:
TiAl, Intermediate Layer, Adhesion Strength, TiAlN Coatings, Arc Ion Deposition (AIP).

Corresponding author: Song Hyok Han

ABSTRACT

TiAlN coated carbide tools prepared by arc ion deposition (AIP) can be applied to high-speed, full-dry and semi-dry cutting due to their high thermal oxidation resistance and high wear resistance and low friction coefficient, which can greatly increase productivity. To improve the adhesion strength of TiAlN films, a TiAl intermediate layer was introduced between the substrate and the TiAlNcoating, and the effect of the thickness of the intermediate layer on the adhesion strength of TiAlN films was simulated and experimentally verified. Three-dimensional models of TiAlN coated tools were developed to reflect the actual operating conditions and the simulation on the stresses occurred in the intermediate layer under bending loads and thermal loads was carried out through the finite element analysis software ANSYS 19.0. The whole model was constructed for different intermediate layer thicknesses, respectively, and the stresses and strains generated in the intermediate layer were analyzed through simulations. The stress distribution values obtained from the simulation results were compared with the experimental adhesion strength results and the relationship between the stress occurred in the intermediate layer and the adhesion strength was analyzed. The maximum adhesion strength of the coating was 42.7 N for interlayer thickness of W = 0.8㎛, while the bending stress occurring in the considered region at different load conditions (mechanical and thermal loading) was 24.7 MPa, thermal stress 390 GPa and thermal strain 460㎛ were minimized

Citation: Song Hyok Han, Chen Nam Kim, Hyon Gyu Pak, Nam Chol Yu. 2025. "Effect of TiAl Intermediate Layer on the Adhesion Strength of TiAlN Coatings Prepared by Arc Ion Deposition (AIP)", *International Journal of Recent Advances in Multidisciplinary Research,* 12,(12), 12018-12021.

INTRODUCTION

TiAlNcoated carbide tools have attracted much attention due to their high thermal oxidation resistance (900 °C), high hardness, high wearing and heatingresistance [1-4], and have been recognized as excellent tools in high-speed dry machining [5]. Vacuum arc deposition (AIP) technique is one of the most promising physical vapor deposition (PVD) methods for industrial applications of TiAlN coating fabrication due to its high degree of ionization, easy control of parameter values and high deposition rate [6]. Vacuum arc deposition technologies,it is an effective PVD method to produce hard coatings with high hardness, high adhesion and high wear resistance, and many studies have been carried out to fabricate TiAlN coated tools by this method, but different results have been reported due to the difficult fabrication equipment and deposition parameters. Up to now, TiAlN coatings have been successfully deposited on steel [7] and hard alloy substrates [8-10] by the AIP method, but after the TiAlN coatings which have been deposited by the AIP method, damage and internal defects occur due to the different hardness and thermal characteristics of the substrates and coatings [11]. In order to improve the properties of TiAlN coatings, there are many active studies to increase the adhesion strength and hardness of the coatings by applying a pulse voltage between the substrate and the cathode [12, 13]. In order to improve the adhesion strength of TiAlN coatings, an intermediate layer, including Ti and TiAl, is deposited between the substrate and TiAlN coatings to enhance the adhesion strength [14-20]. However, the relationship between the intermediate layer and the TiAlN coating is still unclear because of the difficult parameters of the intermediate layer deposition and the lack of detailed data. In this paper, the effect of the thickness of the intermediate layer of TiAlN on the adhesion strength of TiAlN coatings with different thicknesses on high-speed steel (HSS) substrates was simulated and compared with the experimental results by the AIP method. Three-dimensional models of different thicknesses (0.2~1㎛) were constructed, the stresses and strains developed in the intermediate layer of TiAl under different loadings (mechanical bending, mechanical polarization and thermal loading) were calculated through simulation, and the tool properties and adhesion strength of the coatings were predicted.

Simulation and Experiment

- Modeling and Simulation
- Modeling

The following equation 1 shows thermodynamics which is solved for heat conduction and convection phenomenon during simulation.

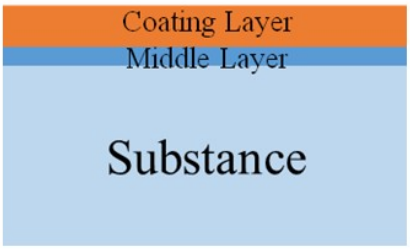

Fig. 1. Structure of the specimen

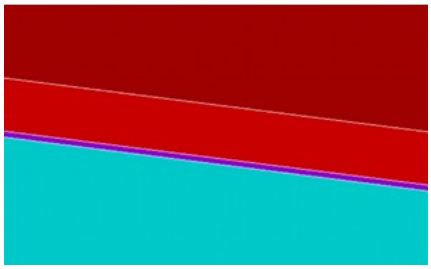

Fig. 2. Three-dimensional model of the sample (red-TiAlN coating, purple-TiAl intermediate layer, green-high-speed steel substrate)

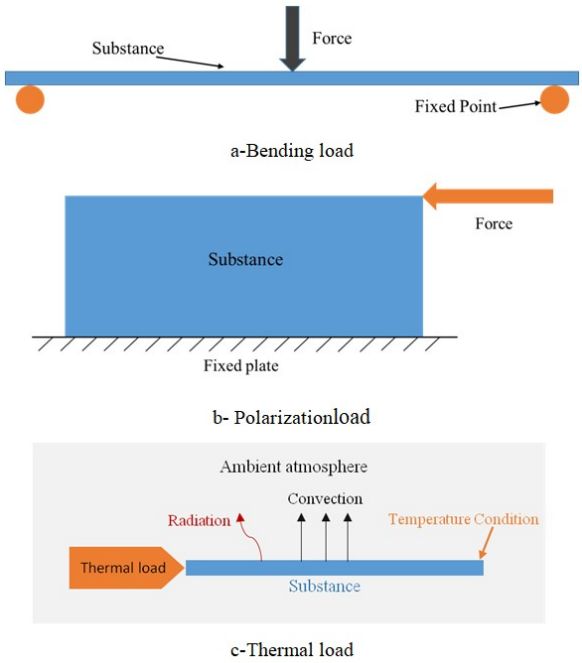

Fig. 3. Bending load, deflection load and thermal load conditions

$$\rho c\left(\frac{\partial T}{\partial t}+\{v\}^T\{L\}^T\right)+\{L\}^T\{q\}=\ddot{q} \quad (1)$$

were,ρ=density, c=specific heat, T=temperature, t=time, $\{q\}$=heat flux vector, $\ddot{q}$=heat generation rate per unit volume, also $\{L\}=\begin{Bmatrix}\frac{\partial}{\partial x}\\ \frac{\partial}{\partial y}\\ \frac{\partial}{\partial z}\end{Bmatrix}$: vector operator

and$\{v\}=\begin{Bmatrix}v_x\\ v_x\\ v_x\end{Bmatrix}$: velocity vector for mass transport of heat.

The vector potential method is implemented in analysis of 3-D electromagnetic fields is discussed in this paper. Considering static and dynamic fields, the following subset of Maxwell's equations (from equation 2 to 4) apply:

$$\nabla\times\{H\}=\{J\}(2)$$
$$\nabla\times\{E\}=-\frac{\partial B}{\partial t}(3)$$
$$\nabla\cdot\{B\}=0(4)$$

Also, the following equation computes element integration point strains and stresses.

$$\{\varepsilon^{el}\}=[B]\{u\}-\{\varepsilon^{th}\}(5)$$
$$\{\sigma\}=[D]\{\varepsilon^{th}\}\quad(6)$$

where:

$\{\varepsilon^{el}\}$= strains that cause stresses (output as EPEL)
[B] = strain-displacement matrix evaluated at integration point
{u} = nodal displacement vector
$\{\varepsilon^{th}\}$ = thermal strain vector
{σ} = stress vector (output as S)
[D] = elasticity matrix

Simulation: Fig. 4 shows the stress distribution in the intermediate layer when the center is loaded with a force of 50 N under confinement with displacement *dX* = *dY*= *dZ*= 0, as shown in Fig. 3-a for the whole model including the substrate, the intermediate layer and the coating when the thickness of the intermediate layer is W = 0.2, 0.4, 0.6, 0.8, and 1 ㎛, respectively.

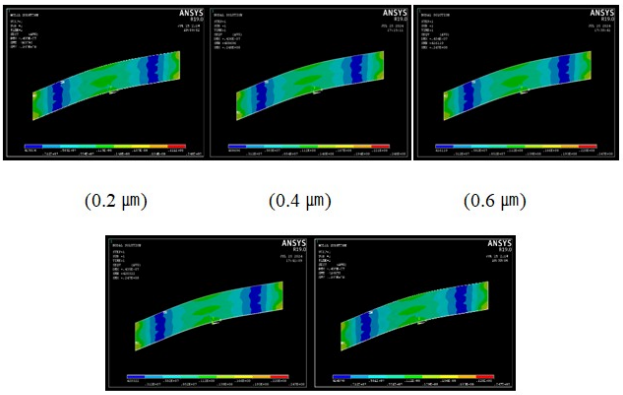

Fig. 4. Images of mechanical stress simulation during bending load application for intermediate layers of different thicknesses

In the figure, red represents the maximum value of compressive stress and blue represents the maximum value of tensile stress. The stress distribution pattern appeared similar, but the detailed stress values were different. When W = 0.2 and 0.4 ㎛, the maximum values of compressive stress occurred relatively large at 24.8 MPa, while when W = 0.6, 0.8 and 1 ㎛, there was a slight decrease at 24.7 MPa. This is because the thickness change of the intermediate layer has little effect on the compressive stress due to the very small ratio of the intermediate layer thickness to the whole model. In the intermediate layer, the compressive stress area was found to be superior to the tensile stress, which is expected to weaken the tensile strain which is detrimental to adhesion when the tool is subjected to bending. The variation of the tensile stress values showed a slight increase as the thickness of the intermediate layer increased, while the compressive stress was only 0.15%. The maximum value of tensile stress for W = 0.2㎛ and the maximum ratio of tensile stress for W = 1 ㎛ are fine, about 1.004 times.

The increase in tensile stress with increasing intermediate layer thickness is associated with an increase in the resistance of the intermediate layer to bending, but the change is expected to have little effect on the overall adhesion due to the slight change. Overall, the influence of the intermediate layer thickness under bending conditions can be considered to be relatively slight.

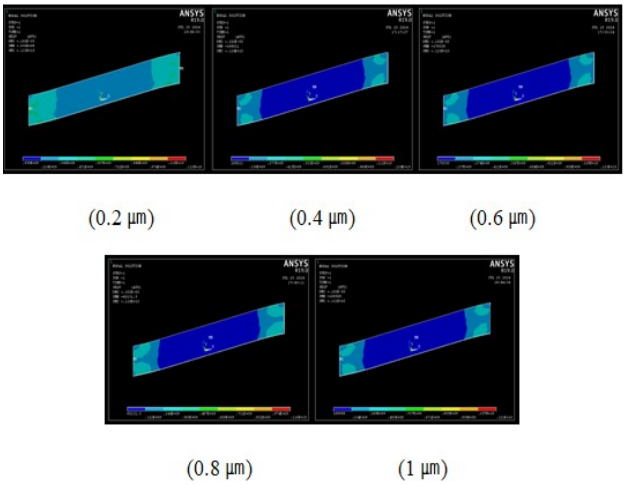

Fig. 5. Image of mechanical stress simulation under bending force loading for intermediate layers of different thicknesses

Fig. 5 shows the stress distribution generated in the middle layer under the applied deflection load (F = 100 N) on the tool model. When W = 0.2 μm, the stress distribution pattern was distinct from the other cases, when the compressive stress prevailed in almost all sides of the intermediate layer. In addition, when W = 0.4, 0.6, 0.8, and 1 μm, the tensile stress dominated the compressive stress. For the concrete stress values, the compressive and tensile stress values were minimized when W = 0.8μm. The maximum values of compressive and tensile stresses generated in the intermediate layer under the bending load are shown in Fig. 6.

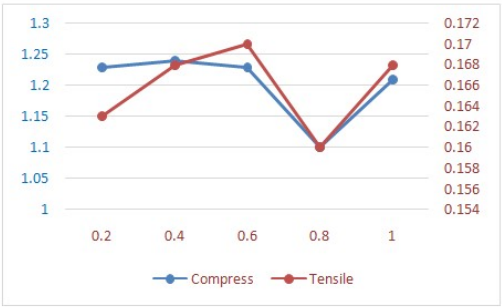

Fig. 6. Maximum curves of compressive and tensile stresses at different intermediate layer thicknesses under shear loading.

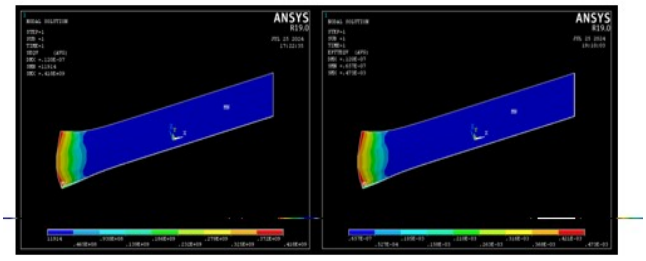

Fig. 7. Thermal stress simulation during thermal loading and thermal strain simulation (at 0.2 thickness of intermediate layer)

Fig. 7 shows the thermal stresses and strains generated by the application of thermal load at W = 0.2μm. The temperature conditions of 900 ◦ C at the left end are given at the right end at 30 ℃ and the heat transfer coefficient, heat capacity, thermal expansion coefficient and thermal radiation conditions for the three layers are given in Table 1. The convective boundary conditions of the atmosphere were neglected. As the thickness of the intermediate layer changes, the thermal stress and strain distribution patterns generated in the intermediate layer are constant and only the specific values are different.

The red region in Fig. 7 is the maximum thermal stress region and the maximum, and these two patterns are very similar. The maximum thermal stress values and maximum strain curves generated are shown in Fig. 8.

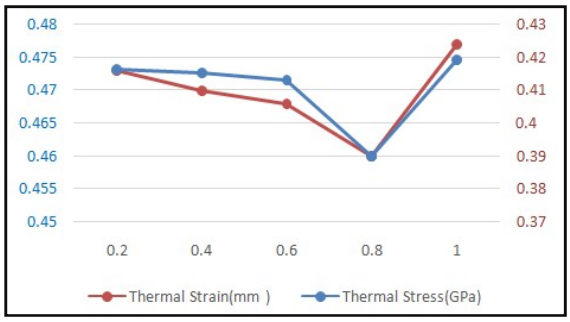

Fig. 8. Thermal stress and thermal deformation curves for different intermediate layer thicknesses under thermal loading

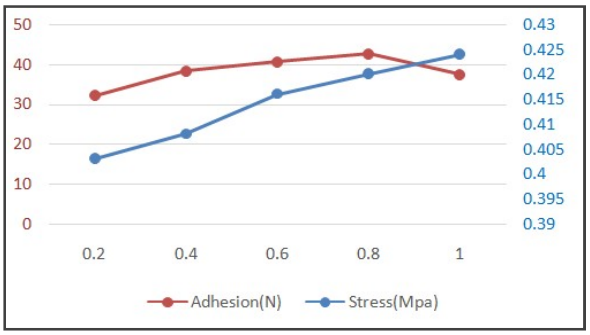

Fig. 9. Comparison of the experimental bond strength with the mechanical stress of the intermediate layer obtained by simulation with bending loads for different intermediate layer thicknesses

As shown in Fig. 8, both thermal stress and thermal strain tended to decrease with increasing intermediate layer thickness, but again increasing with a minimum at w = 0.8 μm. The decrease in thermal stress and thermal strain can be attributed to the fact that the thermal expansion coefficient of the intermediate layer is 9.4×10^{-6}℃$^{-1}$, which belongs to the intermediate value of the substrate and the coating layer, and thus acts as a kind of buffer. However, as the thickness of the intermediate layer continues to increase to more than 0.8 μm, the intermediate layer is considered to be a bulk hexahedron rather than a thin film, which is expected to reduce the bond strength due to the stress concentration inside the intermediate layer due to the different strains at the lower surface where the substrate is attached and at the top surface where the coating is attached.

High-speed steel plates (25 mm × 10 mm × 5 mm) with HRC 62 hardness and Ra = 0.6 mm surface roughness were prepared from the evaporated samples. For TiAlN coatings, a multi-electrode vacuum arc physical coating device LD800 with a maximum reaching vacuum of 8×10^{-4}Pa and a high vacuum reaching time of 40 min was used.
The target material was TiAl (99.99%) with a Ti (99.99%) to Ti:Al ratio of 33:67 (at.%) and Ar (99.99%) and N_2 (99.99%) with working gas. After ultrasonic cleaning for 10 min in the combined washing solution, the samples were air-dried at 100 ◦ C and then placed in the vacuum chamber of the coater. In the experiments, the thickness of the TiAl intermediate layer was 0.2, 0.4, 0.6, 0.8, and 1μm. The deposition parameters for TiAlN coatings are listed in Table 2. The adhesion strength of TiAlN coatings was measured by an automatic scratch tester (CSEM Revetest). The loading rate of the automatic scratch tester was 100 N/min, the scratching rate was 10 mm/min, and more than three measurements were performed for each sample, and the measured values were averaged to evaluate the bond strength.

Table 1. Material properties used in thermal simulations

Parameter / Item	Thermal Conductivity (W/m°C)	Thermal Capacity (J/kg°C)	Coefficient of Thermal Expansion ($°C^{-1}$)	Thermal Radiation rate
Substrate (high-speed steel)	61	1000	1.2×10^{-5}	0.3
Intermediate layer (TiAl)	25	830	9.4×10^{-6}	-
Coating (TiAlN)	21.9	800	9×10^{-6}	0.6

Table 2. Process-specific deposition parameters for TiAlN coatings

Process	Pressure (Pa)	Ar (sccm)	N_2 (sccm)	Bias (V)	Target	Current (A)	Temperature (°C)	Time (min)	Thikness (μm)
Ar-ion washing		600		1000			400	10	
Ti-target	0.05			800	Ti	80		1	
TiAl-target	0.05			800	TiAl	80		1	
Ti-transient layer		10		150	Ti	50	200	2	
TiAl-intermediate layer		10		150	TiAl	60	200		0.2~1
TiAlN-coating			500	100	TiAl	60	200	40	3.2

RESULTS AND DISCUSSES

As shown in Fig. 9, the tensile stress developed in the intermediate layer continues to increase as the intermediate layer thickness increases, but the bond strength shows a maximum value (42.7 N) when the intermediate layer thickness is 0.8 μm. The continuing increase in tensile stress is due to the thicker intermediate layer for the same bending force, which causes more load to be applied here, and thus the relative slip with the TiAlN film increases. The observed adhesion strength was 42.7 N, which could be attributed to the good adhesion of the TiAl intermediate layer to the Ti layer, and further to the diffusion of nitrogen from the TiAlN coating to the intermediate layer, leading to a stronger adhesion. As the thickness of the intermediate layer increases, the bond strength decreases, which is attributed to the weakening of the hardening effect of impurities in the solid solution in the thicker TiAl intermediate layer, which increases the possibility of shear rupture in the intermediate layer.

CONCLUSION

To improve the adhesion strength of the TiAlN film, a TiAl intermediate layer was introduced between the substrate and the film, and the effect of the thickness of the intermediate layer on the adhesion strength of the TiAlN film was simulated and experimentally verified. The following conclusions are drawn from the simulations and experiments. *First*, with the increase of the thickness of the intermediate layer under bending loading, the mechanical stress tended to continue to increase slightly, so that the effect of tool deformation during work would be very small. *Secondly*, the mechanical stress was minimized when W = 0.8 μm was applied to the tool with a deflection load. *Thirdly*, when the thermal load was applied, both the thermal stress and the thermal strain at W = 0.8 μm also exhibited minimum values. *Fourth*, the adhesion strength was measured experimentally with a maximum value of W = 0.8μm. Summarizing the above results, the simulation and experimental results agree very well, indicating that W = 0.8 μmis a reasonable thickness of the intermediate layer. In other words, the deposition of TiAlN coating after 0.8μm of TiAl intermediate layer can not only increase the adhesion strength between the coating and the substrate, but also ensure the tool life.

REFERENCES

Habig, K.H. G.M.Z. Kocker, 1993. Surf. Coat. Technol. 62 428.

Konig, W. R. Fritsch, D. Kammermeier, 1991. Surf. Coat. Technol. 49 316.

Hofmann, D. B. Hensel, M. Yasuoka, N. Kato, 1993. Surf. Coat. Technol. 61 326.

Molarius, J.M., A.S. Korhonen, E. Harju, R. Lappalainen,1987. Surf. Coat. Technol. 33 117.

Wang, D.Y. Y.W. Li, W.Y. Ho, 1999. Surf. Coat. Technol. 114 109.

Li, M.S. F.H. Wang, Surf. 2003. Coat. Technol. 167 197.

Zhiqiang Zhang, Lan Zhang, Heng Yuan et.al. 2022. Tribological Behaviors of Super-Hard TiAlN Coatings Deposited by Filtered Cathode Vacuum Arc Deposition, Materials 15, 2236. https://doi.org/10.3390/ma15062236

Anderbouhr, S. V. Ghetta, E. Blanquet, C. Chabrol, F. Schuster, C. Bernard, R. Madar, 1999. Surf. Coat. Technol. 115 103.

Wang, Y.K. X.Y. Cheng, W.M. Wang, X.H. Gu, L.F. Xia, T.C. Lei, W.H. Liu, 1995. Surf. Coat. Technol. 72 71.

Cheng, Y.H. B.K. Tay, S.P. Lau, X. Shi, H.C. Chua,2000. Thin Solid Films 379 76.

Navinšek, B. P. Panjan, J. Krušič, 1998. Surf. Coat. Technol. 98 809.

Keunecke, M. , C. Stein, K. 2010. Bewilogua Modified TiAlN coatings prepared by dc pulsed magnetron sputtering, Surface & Coatings Technology 205 1273–1278

Bujak J. *et al*., 2004. Surface and Coatings Technology,(180-181); 150-157.

Zhao S. S. *et al*., 2008. Surface and Coatings Technology,(202); 5170-5174.

Wang M. M. *et al*., 2015. Vacuum, (52), 1; 34-38.

Yang G. Y. *et al*., 2017. Rare Met.,(36), 8; 651-658.

Lugscheider E. *et al*., Surface and Coatings Technology, 1995(76-77); 700-705.

Lii D. F. *et al*., 1998. Surface and Coatings Technology,(99); 197-202.

Lin W. *et al*., 2018. Ceramics International, (44); 2209-2215.

Gamal S.H. *et al*., 1990. Carrier lifetime measurement by ramp recovery of p-i-n diodes, IEEE Trans. Electron Devices, vol. 37, pp. 1921-1924,

Jonsson, P. M. Isberg, M. Rosling, H. Bleichner, and E. Nordlander, An Improved Technique for Ambipolar Carrier-Lifetime Extraction in Low-Doped Silicon (Internal Report).

Rosling, M. H. Bleichner, and E. Nordlander, 1991. Symposium on Materials and Devices for Power Electronics, Proc. MADEP '91, pp. 59-64.

Baliga, B. J. 2008. Fundamentals of Power Semiconductor Devices, pp. 24-84

Marina Valdinoci *et al*., 1996. Analysis of Conductivity Degradation in Gold/Platinum-Doped Silicon, IEEE transactions on electron devices, VOL. 43, NO. 12, DECEMBER

Dieter K. Schroder, 1997. Carrier Lifetimes in Silicon, IEEE Transactions on electron devices, vol. 44, no. 1, january

Ingo Dimstorfer *et al*., 2014. Near surface inversion layer recombination in Al_2O_3passivatedn-type silicon, Journal of Applied Physics 116, 044112

****